Automated Action Generation based on Action Field for Robotic Garment Manipulation

Hu Cheng, *Member, IEEE,* Fuyuki Tokuda, *Member, IEEE,* Kazuhiro Kosuge, *Life Fellow, IEEE*

arXiv:2505.03537v1 [cs.RO] 6 May 2025

***Abstract*—Garment manipulation using robotic systems is a challenging task due to the diverse shapes and deformable nature of fabric. In this paper, we propose a novel method for robotic garment manipulation that significantly improves the accuracy while reducing computational time compared to previous approaches. Our method features an action generator that directly interprets scene images and generates pixel-wise end-effector action vectors using a neural network. The network also predicts a manipulation score map that ranks potential actions, allowing the system to select the most effective action. Extensive simulation experiments demonstrate that our method achieves higher unfolding and alignment performances and faster computation time than previous approaches. Real-world experiments show that the proposed method generalizes well to different garment types and successfully flattens garments.**

***Note to Practitioners*—Vision-based robotic garment manipulation faces significant complexities due to garments' diverse shapes and high-dimensional states, which pose challenges for both state perception and action generation. In this paper, we propose a novel deep neural network that can generate actions to unfold various garments from their RGB images. Compared to existing methods, our method generates pixel-level actions across the entire garment area, each providing a predicted manipulation score that assists in the selection of a final manipulation action. In addition, the generation requires only a single-shot network forward computation, which significantly improves efficiency. The training data consists of large-scale recorded garment state parameters and the corresponding manipulating actions in the simulator. Real-world experiments demonstrate the effectiveness and generalization capability of our model.**

***Index Terms*—Robotic garment manipulation, vision-based perception, action generation.**

I. Introduction

ROBOTIC manipulation of deformable objects is essential in various applications, such as cable routing [1], bag opening [2], and garment manipulation [3]–[5]. Among these, garment and fabric manipulation present unique challenges due to their high degrees of freedom, self-occlusion, and complex nonlinear material properties. These characteristics make it difficult to estimate the state of the fabric and generate actions for manipulators. To address these challenges, vision-based deep learning methods have been explored. These methods can be generally categorized into two groups: one is the two-stage method that first estimates the fabric state and then heuristically generates actions based on the state; the other one is the single-stage method, which directly outputs action from the visual input.

Hu Cheng and Fuyuki Tokuda are with the Department of Electrical and Electronic Engineering, The University of Hong Kong, Hong Kong, and also with the InnoHK Centre for Transformative Garment Production, Hong Kong (email: hucheng@hku.hk, fuyuki.tokuda@transgp.hk).

Kazuhiro Kosuge is with the JC STEM Laboratory of Robotics for Soft Materials, Department of Electrical and Electronic Engineering, The University of Hong Kong, Hong Kong, and also with the InnoHK Centre for Transformative Garment Production, Hong Kong (e-mail:kosuge@hku.hk).

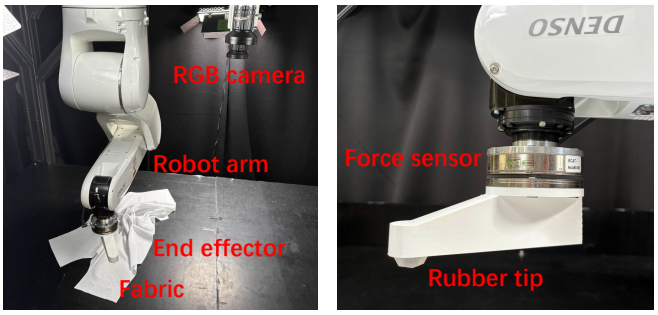

(a) Robot Platform (b) End-effector

Fig. 1: (a) is the robot platform and (b) shows the end-effector used to manipulate the fabric.

The performance of two-stage methods depends heavily on the accuracy of fabric state estimation, which is often computationally expensive and sensitive to self-occlusion. Several techniques, such as dense visual correspondences by Ha and Song [6], garment mesh modeling by Chi and Song [7], and semantic keypoint extraction by Deng and Hsu [8], have been introduced to improve garment state estimation. While these methods have significantly advanced the accuracy and robustness of garment state estimation, challenges remain in handling complex deformations and occlusions.

Single-stage methods [9]–[12] directly output the garment manipulation action from visual observations, which eliminates the need for explicit fabric state estimation and simplifies the action generation. These methods have proven effective in various manipulation tasks and have contributed to simplifying the action generation compared to the two-stage methods. However, many single-stage approaches rely on the spatial action map strategy [13], which involves multiple feed-forward of the network and often represents flattening actions such as the pulling direction and pulling distance in predefined and discretized values. The details of the related research are further presented in Section II.

In this paper, we propose a novel learning-based action-generation framework that directly interprets scene images and generates the manipulation score, distance, and angle maps, simultaneously. These maps are then converted to pixel-wise end-effector action vectors, i.e., action field. By representing the manipulator's action as pixel-wise end-effector action vectors, our method only requires a single forward propagation of the network to generate an action of the manipulator. Our approach improves the accuracy and efficiency of garment

manipulation compared to the previous method.

We propose a robotic garment and fabric manipulation system as shown in Fig. 1(a), which accomplishes the unfolding and positioning of different garments through planar actions by a low-cost and robust single-tip end-effector. The main contributions are summarized as follows:

- The proposed method consists of an action generation method that can directly generate pixel-wise action field from the image of a crumpled garment, significantly increasing efficiency compared to the existing single-stage garment manipulation method.
- We claim that the score map training suffers from the class imbalance, and propose to incorporate the semantic information of the garment to address this issue. In addition, we leverage the action field representation and propose a novel training scheme named *shape loss* to supervise the learning of the distance and angle map.
- Extensive simulation experiments demonstrate that our method achieves a higher coverage index and alignment index and faster computation time than previous approaches.
- Real-world experiments further validate the robustness of our approach, showing that the proposed method generalizes well to different garment types and successfully flattens garments.

In the following, Section II presents related work for the deformable object manipulation. Section III explains the action generator structure and training modules. Section IV presents the experimental results and ablation studies. Section V concludes this paper.

II. Related Work

The vision-based deformable object manipulation policy depends on the state perception methods and the action generator strategy. In this section, we first introduce state representations used in the two-stage methods. Then, we introduce single-stage methods based on the spatial action map strategy.

A. State Representations in Two-Stage Methods

1) Visual correspondence: Visual correspondence is the process of finding a mapping between pixels in two or more images that correspond to the same surface point on an object. Initially, it was designed for rigid objects in tasks such as pose estimation [14] and object manipulation [15]. Sundaresan *et al.* [6] proposed a dense (pixel-wise) visual correspondence for a highly deformable rope to perform robot knot-tying, and later extended the similar technique to fabric smoothing and unfolding [16]. The dense (pixel-wise) visual correspondence can be used to generate a fabric manipulation policy through heuristic rules, but the computational cost tends to be high.

To reduce computational cost and improve robustness, some works propose sparse visual correspondence that uses specific keypoints for visual correspondence. Deng *et al.* [8] extracted semantic keypoints within garments, and Wu *et al.* [17] established correspondences between keypoints of different garments with identical topological structures. Although sparse visual correspondence improves computational efficiency, it represents the fabric state in a discretized form [18], [19]. This makes it hard to capture small wrinkles or subtle shape changes of the fabric. Also, these methods often depend on hand-crafted features and rule-based policies, which can limit their ability to handle different types of garments [20].

2) 3D reconstruction: Another approach for state representation of the fabric is based on 3D reconstruction. Those works are proposed to estimate the complete geometric configurations of fabric from RGB or depth sensors. Lin *et al.* [21] and Wang *et al.* [22] modeled the fabric using Graph Neural Networks (GNNs), while Chen *et al.* [7] estimated a full 3D mesh in a canonical frame through mesh-completion techniques. Huang *et al.* [23] progressively reconstructed the garment mesh from a single depth image. While the reconstructed mesh state enables heuristic policy generation, it typically involves high computational overhead.

3) Key region detection: Other methods for garment state representation use key region detection approaches that focus on identifying geometric or semantic regions of interest rather than individual keypoints. Raval *et al.* [24] used a traditional corner detector [25] to detect garment corners, and integrated a foundation model [26] as a high-level planner for garment smoothing and folding. Clark *et al.* [27] classified garment edges into different categories to guide manipulation. Others extracted regions of interest such as collars [28] and bag handles or rims [2]. These methods achieve higher computational efficiency by focusing on specific semantic regions. However, they often lose detailed geometric information and rely on hand-crafted features. Consequently, the policies are typically designed with task-specific rules, which can limit generalization across diverse garment types.

4) Optical-Flow-Like representation: Another type of two-stage framework uses optical-flow-like descriptors to unify state estimation and policy generation. Weng *et al.* [29] proposed to learn cloth-folding actions using a flow map generated from the current and goal images. An auxiliary network selects the pick point, and placement point is inferred based on the flow map. Agarwal *et al.* [30] extended this concept by computing 3D point-cloud correspondences.

The proposed shape loss employs a representation format similar to the flow map. However, it is based on fundamentally different objectives and is regarded as a training procedure. Specifically, the shape loss is computed as the image-level difference between the predefined target state and the state resulting from applying the generated action to the current configuration. This loss serves as a supervisory signal, evaluating how effectively the predicted dense actions deform the garment toward the target shape. Incorporating the shape loss accelerates alignment during the early manipulation stages and leads to improved final accuracy in garment alignment tasks.

B. Single-Stage Methods with Spatial Action Map

The single-stage methods avoid establishing descriptors of deformable objects by generating actions directly from raw sensory observations. The spatial action map was initially proposed to predict a single-channel reward map that indicates the most suitable manipulation point [13] or moving target

[31] for accomplishing a given task. This approach was later extended to infer more complex action configurations, such as the pulling direction and distance required for flattening fabrics, as demonstrated in [9], [32].

The methods proposed in [9], [32] apply a set of predefined transformations to the input image such as image rotations and scaling, and perform a forward pass of the network for each transformed variant to generate corresponding reward maps. The transformation yielding the highest reward value is then selected. The pulling start point is computed by inverting the selected transformation, and the associated transformation parameters (e.g., rotation angle and scale factor) are interpreted as the pulling direction and distance. This strategy has been widely adopted in garment manipulation [10], [11], [33] and plastic bag knotting tasks [34].

However, the spatial action map approach is computationally intensive, as it requires multiple forward passes of the network for each rotated and scaled input image. Furthermore, because action parameters such as pulling direction and distance are sampled from a discrete set, the selected action may not be globally optimal. In contrast, our method predicts pixel-wise action maps with continuous values for score, pulling direction, and distance in a single forward pass, enabling more efficient and precise action generation.

III. Methodology

In this section, we first describe how we define the planar robot action that manipulates fabrics. Then, we elaborate on the structure of the action generation network and the corresponding design of the loss function. Finally, we present the details of the collected training data.

A. Action Representations

In this paper, we consider a task in which a robot manipulates a garment using planar sliding actions. The objective consists of two subtasks: (1) flattening the garment to eliminate wrinkles and increase its coverage area, and (2) aligning the garment to a predefined target pose with the desired position and orientation. Both subtasks are achieved through a sequence of planar actions executed by a simple single-tip end-effector. The end-effector with a rubber tip is attached to the manipulator as shown in Fig. 1(b). The rubber tips exhibit high friction against the fabric, whereas the friction between the fabric and the table is relatively low. For this planar action, we define it using a 4D vector: $[x, y, \theta, d]$, as shown in Fig. 2(a). The starting point (x, y) is the initial contact position in image space where the end-effector first presses down the fabric. A downward force is then applied to press the fabric firmly against the table, ensuring stable contact during the action. Finally, the robot arm moves along a straight path in the direction of angle θ with a distance of d. This action causes the fabric to slide on the table surface and unfold the fabric, as shown in Fig. 2(b).

B. Action Generator

Based on the action definition in Section III-A, we design a dense action generator for garment manipulation, as depicted in Fig. 3. The model's input is the captured RGB image of the garment or fabric, which is processed by an encoder-decoder to extract features. The output head then produces a 3-channel image that represents the action of the manipulator. Each pixel in the output corresponds to a robot action, with the three channels indicating the action's score, direction, and distance. Using this 3-channel image, we can construct a pixel-wise action field as shown in Fig. 3.

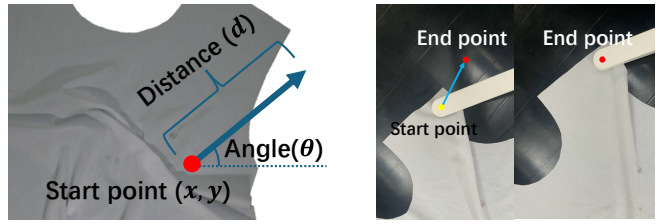

(a) Action definition (b) Action effect

Fig. 2: (a) The action that manipulates the fabric contains the start point (x, y) in the image, the moving distance d, and the moving angle θ. (b) demonstrates the sliding effect of the fabric by applying the action.

1) Model backbone: The input of the model consists of an RGB image. The features are then extracted using a ResNet-18 [35] backbone, which functions as the encoder $\mathbf{E}$. The feature maps from different stages of ResNet-18 are then upscaled and progressively concatenated to match the resolution of the input images. This process forms the decoder $\mathbf{D}$, which provides feature maps enriched with both semantic information and fine-grained details, essential for the output head. The $\mathbf{E}$ and $\mathbf{D}$ constitute the model backbone, as shown in Fig. 3.

2) Output heads: The output head is attached to the last-stage feature maps of the model backbone to generate a 3-channel image. Each distinct channel corresponds to a different aspect of the action. The score map indicates the possibility of a pixel location being the start point of the action, the angle and distance map specify the moving direction and magnitude of the action, respectively. By combining the pixel values from these three channels at the same location, a manipulation action can be determined.

a) Score head: The score head is constructed by three stages of cascaded layers: the fully convolutional layer, the ReLU layer, and the Squeeze-and-Excitation block (SEBlock) [36]. While the former two layers are used to integrate features effectively, SEBlock is introduced to enhance the score map head by recalibrating channel-wise responses. This helps the model focus on more relevant features and improves feature discrimination without the need for additional regularization layers. As a result, the network achieves precise localization of high-score regions that are suitable for unfolding or aligning the fabric.

The architecture of each stage in the score map head is noted as:

$$\text{Conv2d}(\mathrm{C}_{i-1}, \mathrm{C}_i, kernel = 3) \;\rightarrow\; \text{ReLU} \;\rightarrow\; \text{SEBlock}(\mathrm{C}_i),$$

where $C_\times$ represents the channel number of the feature maps,

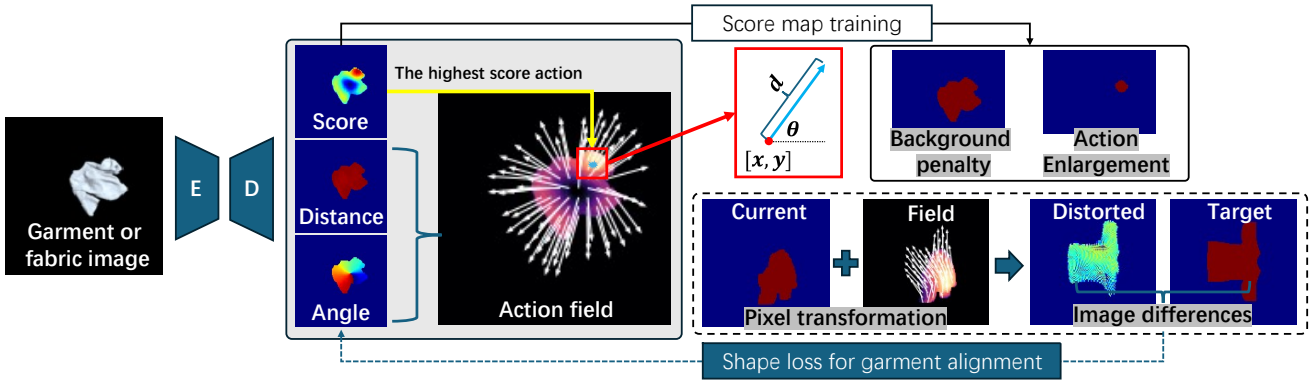

Fig. 3: Framework of the proposed dense action generator.

and the kernel size of the 2D convolutional layer is $kernel = 3$. Here, i denotes the stage index in the score map head.

b) Distance head: The moving distance of the end-effector d is calculated by multiplying the base unit d_b (in pixels) with a scale factor s:

$$d = s \times d_b. \tag{1}$$

The scale factor s is defined as:

$$s = d_{\text{scale}} \cdot \text{sigmoid}(x) + d_{\text{offset}}, \tag{2}$$

where x is the output of the distance head. d_{scale} and d_{offset} are used to linearly scale and shift the sigmoid function. This formulation constrains s within a certain range, ensuring that the calculated distance remains within the robot's physical limitations and operational workspace, as long as d_b, d_{scale}, and d_{offset} are selected appropriately. In the experiments presented in Section IV, $d_b = 10$, $d_{\text{scale}} = 2.75$, and $d_{\text{offset}} = 0.25$ are chosen.

c) Angle head: For the angle map, we split the predicted elements into $\sin\theta$ and $\cos\theta$, to avoid ambiguity of the angle periodicity. The angle prediction head consists of two hidden layers followed by two separate heads with tanh activations. The details of the angle head are as follows:

$$\left.\begin{array}{c}\text{Conv2d}(C_{in}, C_{out}, kernel = 1) \rightarrow \text{ReLU} \\ \downarrow \end{array}\right\} \times 2$$
$$SIN(\theta)\text{: Conv2d}(C_{in}, C_{out} = 1, kernel = 1) \rightarrow \text{Tanh},$$
$$COS(\theta)\text{: Conv2d}(C_{in}, C_{out} = 1, kernel = 1) \rightarrow \text{Tanh}.$$

C. Loss Design

The proposed loss function consists of two components: the score loss, which enables the network to predict a score map for selecting pulling start points, and the angle and distance loss, which guides the network to output pulling directions and distances. Additionally, the shape loss is added as an auxiliary supervision for the alignment task.

1) Score loss: In previous methods [9], [10], [13], they only use a single point score and mask out the others in the regression loss calculation. These methods can easily result in potential overfitting during training, leading to the focus drifting from the foreground area and unintentionally highlighting the background. Consequently, it is important to incorporate additional pixel information, specifically the neighboring pixels surrounding the labeled point within the garment region, into the loss calculation.

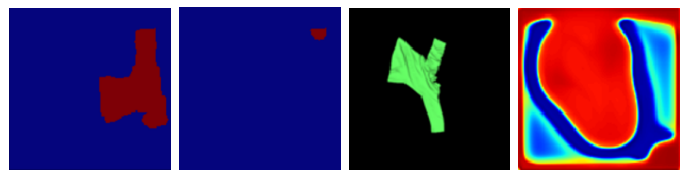

(a) (b) (c) (d)

Fig. 4: (a) shows the garment mask, and (b) shows the enlarged action areas that are filtered by the garment mask. (c) is the input image and (d) is the generated score map without action enlargement, which incorrectly focuses on the background and can not differentiate the areas in the garment or fabric.

Unlike the previous score loss design [9], [10], [13], which only considers a single score value during the sampling, our score loss design incorporates the prior knowledge about robot manipulation of a fabric:

(1) The movement results of fabric manipulation should have consistency within a small local area.
(2) The pulling action should preferably originate within the boundary of the fabric.

These conditions reflect the reality of the fabric manipulation task and also help to improve the score regression performance, particularly in addressing the extreme imbalance issue between the foreground and background pixel numbers. Notably, each training sample includes a score label for only a single pixel in the simulated image.

According to constraint (1), adjacent points on the fabric generally lead to similar manipulation results due to the local homogeneity and continuity of the deformable material. To satisfy constraint (2), the pulling start points should be accurately confined within the garment by applying a segmentation mask (Fig. 4(a)). Based on these considerations, we assign the same score value to the neighboring pixels around the sampled point, as long as they lie within the garment region (Fig. 4(b)). The score is computed based on the difference in the garment's state before and after applying the corresponding action.

We effectively increase the area of the foreground by convolving the mask of the score labeled action area M_{Action}

with a predefined circular kernel K, and then applying binary thresholds to obtain the enlarged action mask $M_{EAction}$:

$$K_{i,j} = \begin{cases} 1 & \text{if } i^2 + j^2 \leq r^2, \text{ for } i, j \in [-r, r] \\ 0 & \text{otherwise} \end{cases},$$
$$M_{EAction} = \begin{cases} 1 & \text{if } (M_{Action} * K) > 0 \\ 0 & \text{otherwise} \end{cases}, \tag{3}$$

where the 2D circular kernel K is with size $(2r+1)\times(2r+1)$, and $r = 3$, and $M_{Action} * K$ denotes the convolution of the action mask M_{Action} with the kernel K. One sample of a $M_{EAaction}$ is shown in Fig. 4(b).

Then, the adjusted loss for action, L_a, is calculated as:

$$L_a = \text{Mean}\Big(\text{SmoothL1Loss}\Big(\tilde{I}_s \odot M_{EAction}, gt_s \cdot M_{EAction}\Big)\Big), \tag{4}$$

where gt_s is a single ground truth score value from the training data, and $\tilde{I}_S$ is the predicted action score map.

Meanwhile, the score map (Fig. 4(d)) generated for the input (Fig. 4(c)) by the single pixel regression erroneously focuses on the background, failing to accurately and clearly segment the garment. Based on this pre-training result and given the constraint (2), the minus scores $gt_b = -1$ are assigned to the background pixels $M_{Background}$, which also guides the training process by penalizing the background areas. The background loss, L_b, is calculated as:

$$L_b = \text{Mean}\Big(\text{SmoothL1Loss}\Big(\tilde{I}_s \odot M_{Background}, gt_b \cdot M_{Background}\Big)\Big). \tag{5}$$

Instead of constraining only a single action point [9], [10], [13], our final score loss includes the regression loss of each pixel from both the enlarged action and background area. Specifically, the score loss L_{score} is the weighted sum of L_a and L_b, whose contribution is adjusted by $\lambda_b = 0.001$. The L_{score} is calculated as:

$$L_{score} = L_a + \lambda_b \cdot L_b. \tag{6}$$

Through these processes, the foreground area is effectively enlarged and the background information is also considered, which helps mitigate overfitting caused by the class imbalance.

2) Angle and distance loss: Both the angle loss L_{angle} and the distance loss L_{distance} are computed by averaging the regression errors between the predicted and ground truth values in the angle map I_A and the distance map I_D. These losses are calculated only at the pixel locations specified by the action mask M_{EAction}.

The angle loss, L_{angle}, based on the angle prediction in Section III-B2c, requires the regression of two corresponding values, $\sin(\theta)$ and $\cos(\theta)$, and a penalty part to regularize them to satisfy the unit circle constraint:

$$L_{sin} = \text{Mean}(\text{SmoothL1Loss}(\tilde{I}_{sin} \odot M_{EAction}, gt_{sin} \cdot M_{EAction})), \tag{7}$$
$$L_{cos} = \text{Mean}(\text{SmoothL1Loss}(\tilde{I}_{cos} \odot M_{EAction}, gt_{cos} \cdot M_{EAction})), \tag{8}$$
$$L_p = \text{Mean}((\tilde{I}_{sin})^2 + (\tilde{I}_{cos})^2 - 1)^2 \odot M_{EAction}), \tag{9}$$
$$L_{angle} = L_{sin} + L_{cos} + \lambda_p L_p, \tag{10}$$

where L_{sin} and L_{cos} are the regression losses for the predicted angle images, $\tilde{I_{sin}}$ and $\tilde{I_{cos}}$, respectively, under the supervision of the triangle values, gt_{sin} and gt_{cos} of the ground truth angle. Finally, the angle regression loss L_{angle} is their weighted sum with the unit norm penalty $L_p = 1.0$ with weight λ_p.

The calculation of the distance loss, $L_{distance}$, is also the regression loss between the predicted distance map, $\tilde{I}_d$, and the labeled ground truth distance values, gt_d:

$$L_{distance} = \text{Mean}\Big(\text{SmoothL1Loss}\Big(\tilde{I}_d \odot M_{EAction}, gt_d \cdot M_{EAction}\Big)\Big), \tag{11}$$

3) Shape loss: In addition to supervising the training with angles and distances labeled by humans or simulators, our model is also supervised using the desired final shape of the garment for the alignment task. The calculation components of the proposed shape loss are shown in Fig. 5.

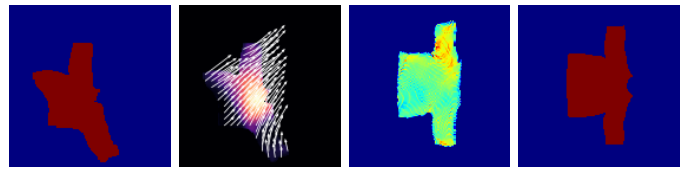

(a) Current state (b) Action field (c) After state (d) Target state

Fig. 5: The state images and the action field involved in calculating the shape loss. (a) shows the mask of the garment in its current state. (b) is the action field determined by the predicted angle and distance map. (c) is the result of applying the dense actions (b) to each pixel in the mask of (a). (d) is the mask representing the target state of the garment in the alignment task.

In the garment alignment task, the final goal is deterministic and can be represented by a garment mask in a predefined, fully flattened pose. Based on the predetermined target state, we propose a novel loss function that compares the discrepancy between the garment mask of the target state I_{target} (Fig. 5(d)) and that of the approximate state $I_{distort}$ (Fig. 5(c)), where $I_{distort}$ is generated through the pixel level transformation based on the densely generated actions.

The predicted angle and distance maps can be combined into a single action field image, as shown in Fig. 5(b). In both simulated and real-world physics, each individual action depicted in Fig. 5(b) cannot independently transform a single point due to the interconnected forces of adjacent points. However, the aggregate effect of these actions can approximate the overall

manipulation results if all points are moved according to all predicted actions. In other words, the overall transformations based on the action field provide valuable insight into the efficacy of the predicted actions, and these transformations can be observed as a displacement field $\mathcal{D}$. $\mathcal{D}$ denotes the horizontal and vertical pixel movement offsets $[\Delta x, \Delta y]$ to formulate a new image. To this end, we propose the shape loss during the training:

$$L_{shape} = MSE(I_{target}, I_{distort}), \tag{12}$$

$$I_{distort} = \mathcal{D}(I_{current}). \tag{13}$$

The shape loss L_{shape} is a classification loss and computed using Mean Squared Error (MSE) to assess the discrepancy between the target mask I_{target} and the distorted image $I_{distort}$. $I_{distort}$ is obtained by applying pixel movements, as determined by $\mathcal{D}$, to $I_{current}$ (Fig. 5(a)), resulting in the distorted image.

4) Total loss: The total loss is the sum of the action score loss and the action parameters regression losses (angle and distance). There is an additional shape loss for alignment tasks.

$$L_{total} = L_{score} + \lambda_a L_{angle} + \lambda_d L_{distance} + \lambda_s L_{shape}, \tag{14}$$

where both λ_a and λ_d are set to 0.1 to balance their contributions. λ_s is set to zero during the unfolding task, and to 25.0 for the alignment task to minimize excessive focus on the target shape, which could lead to overfitting.

D. Data Collection

Considering the high-dimensional nature of the fabric state and the action space, training the model presents significant challenges, requiring a large volume of high-quality data. Thus, we collected the training data in the simulator to avoid tedious human labeling. This process consists of two parts: the simulation of garment dynamics under various actions using a particle-based method, and the rendering process to obtain a highly realistic image based on these particles.

1) Action labeling: All training samples are labeled using simulators described in [9] and [10]. These simulators operate within the deformable object manipulation environment of SoftGym [37], which is based on a wrapper [38] for the particle-based simulator NVIDIA FleX. For the labeling of each sample, we simulate the planar action "pull" defined in Section III-A. The sampled action and the state changes of a garment during the action labeling are shown in Fig. 6. The pulling start position $[x, y]$, the angle θ, and the distance d are all randomly sampled. Considering the restrictions, the position should be within the garment, and the distance should satisfy the physical meaning to match the robot workspace limitation. The labeling process records the state parameters of the garment before and after applying the action, and the changes of these values are attached to the action as its score. Specifically, for the garment unfolding, the system records the coverage index value, which is defined as the ratio of the garment's area in its current state to its area when fully flattened. For the alignment, the alignment index value is recorded and defined as the Intersection over Union (IoU) value between the mask of the garment in its current state and the target state. These coverage and alignment indexes also work as the evaluation metrics for the garment unfolding and alignment experiments, with greater values representing better performance.

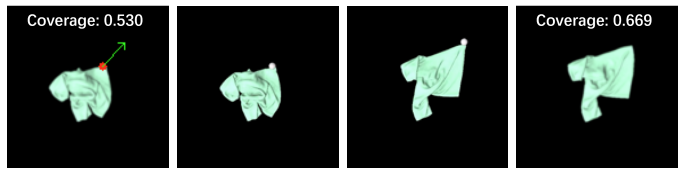

(a) Init state (b) Action start (c) Action end (d) Final state

Fig. 6: The sampled action and the state changes of a garment during the action labeling. (a) shows the current state of the garment, its coverage index score, and the randomly generated actions, with the red dot representing the start point $[x, y]$ and the arrow that is configured by the sampled angle and distance. (b) and (c) depict the start and end state snapshots of attaching the "pull" action, with the end-effector visualized as the gray sphere. (d) presents the final state with the updated coverage index score.

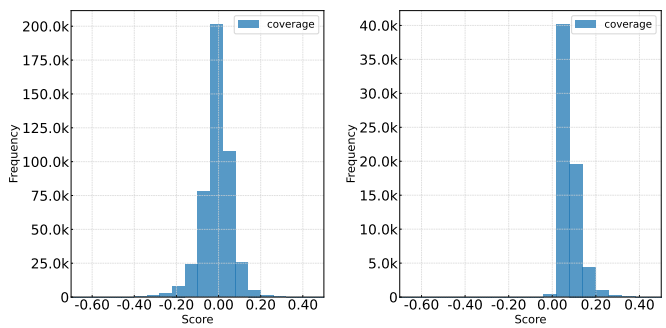

(a) Initial samples (b) Refined samples

Fig. 7: Distributions of the reward score (coverage index) before (a) and after (b) the refining process.

To generate actions densely, our model simultaneously outputs the score, angle, and distance maps, which are mutually independent during training. Because of this independence, we must carefully filter out samples with low or negative reward scores to prevent adverse effects on model training. To this end, we refine the randomly collected samples based on their reward scores. Specifically, the samples are evaluated against a predefined threshold determined by the task objective, such as the coverage index or L2 distance. Changes in the distribution of the dataset are illustrated in Fig. 7. After refining the dataset, all samples with negative values are dropped, and the samples with smaller values are suppressed. As a result, the total number of samples is significantly reduced.

All the training data fed to the model are associated with positive reward scores, meaning the model parameters will only be updated based on the sampled actions that lead toward the goal state. In this way, the model will predict the areas with high reward scores and the corresponding angle and distance.

TABLE I: Evaluation Results on the Unfolding Task

Methods	Coverage	Time (ms)
Cloth Funnels [10]	0.792	186.0
Ours	0.854	22.6

2) Statistic details: Combining the image with the corresponding action configurations and the recorded scores, we present the garment manipulation dataset specially for the "pull" action. Statistically, we generate 65,000 training samples with the "long sleeves" clothing category for the garment unfolding tasks and 27,000 training samples for the alignment tasks. For evaluation purposes, 400 newly generated scenarios per clothing category (long sleeves, pants, skirts, dresses, and jumpsuits) are created, each containing garments in heavily crumpled states.

IV. Experiments

In this section, we first compare our model with the state-of-the-art method using identical simulated environments. In addition, results of real-world experiments are also provided to demonstrate the effectiveness of the proposed method. These results help evaluate the domain gap between the simulated images and the real-world image of the garment or fabric.

A. Dataset Experiments

We evaluate our dense action generator by comparing it with the traditional discrete spatial action mapping method. In those methods, actions are represented by discrete angle and distance values. Specifically, a series of input images is created by applying fixed-step rotations and scalings to the original image. Each transformed image is passed through the model to generate a score map. The transformation that yields the highest score is selected, and its corresponding angle and distance are used as the action parameters. Note that in this paper, all the garments are in heavily crumpled initial states and should be regarded as "Hard" tasks defined in [10], and they are manipulated with the planar action "pull" only.

1) Quantitative results: In Table I, we compare our proposed method with the previous spatial action map approach [10], which adopted factorized objective functions and reported better performance than their previous seminal work [9]. Our method achieves a coverage index value of 0.854, with a relative increase of 7.83% over the previous 0.792, demonstrating its superior performance in garment unfolding and wrinkles elimination. Moreover, the conventional spatial action map method requires multiple forward passes of the model for a sequence of transformed input images. In contrast, our model architecture generates continuous and dense actions as output in a single forward pass. Consequently, our approach operates at 22.6 ms per generation compared to 186.0 ms for the method in [10], significantly improving both efficiency and coverage performance in garment unfolding.

Then, to assess the robustness and generalization of the proposed model, we evaluate its performance on different types of garments using the same model trained exclusively on "long sleeves" samples. The results are presented in Table II. These results indicate that the model exhibits strong generalization capabilities when applied to previously unseen and diverse garment types, achieving effective unfolding outcomes. Among these clothing categories, the "long sleeves", "pants", and "jumpsuit" exhibit nearly identical final coverage index values, which are relatively lower than those for other categories. This discrepancy is likely due to the complexities involved in manipulating sleeves and legs.

TABLE II: Evaluation Results on Unfolding Task for Different Garment Types

Train Set	Test Set	Coverage	Training Sample (No.)	Scene (No.)
Long sleeves	Long sleeves	0.854	65,000	2000 training 400 testing
	Pants	0.855	N/A	400 testing
	Skirt	0.915		
	Dress	0.917		
	Jumpsuit	0.857		

TABLE III: Evaluation Results on the Alignment Task

Methods	IoU
Cloth Funnels [10]	0.535
Ours	0.580

Finally, by incorporating the shape loss, our model achieves the garment alignment task with the same model structure, and returns a higher alignment index, i.e., IoU value, than [10]. The results are presented in Table III.

2) Qualitative results: For the qualitative image results shown in Fig. 8, we present the output images of the model, including score maps (deeper red indicates higher scores), angle maps (deeper red implies larger angle values), and action field visualizations, corresponding to the input images of garments in various states. The score map accurately locates the key region for unfolding, such as the sleeve edge, hem, or neckline, rather than the center areas, which are prone to

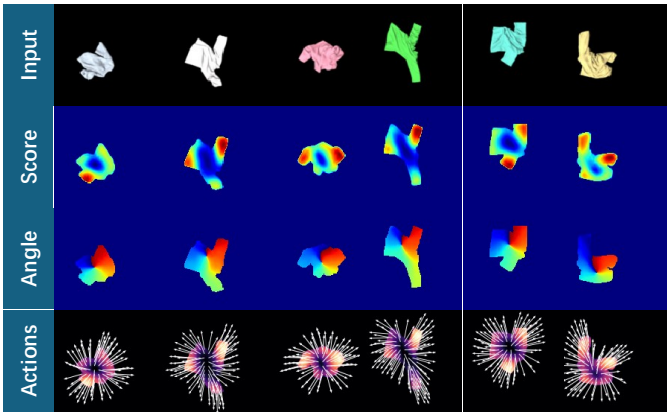

Fig. 8: The visualizations of the score map and dense actions, from top to bottom, are the input, the score map, the angle map, and the generated actions (selected at intervals of 7 pixels) within the garment.

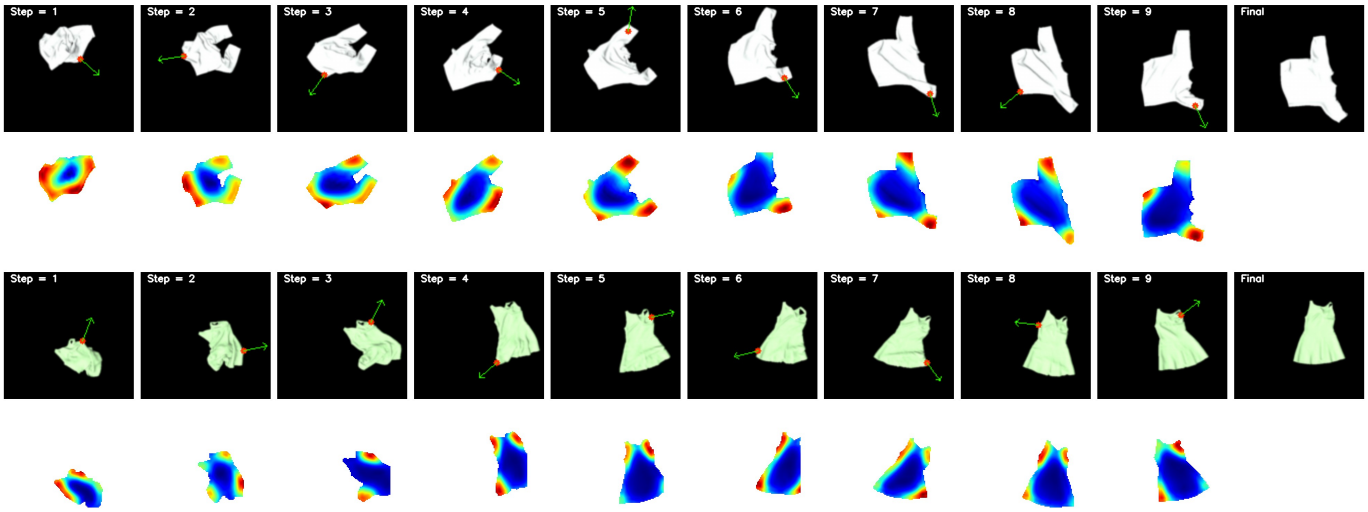

Fig. 9: The step-by-step visualizations of the garment unfolding task of the long sleeves and dress.

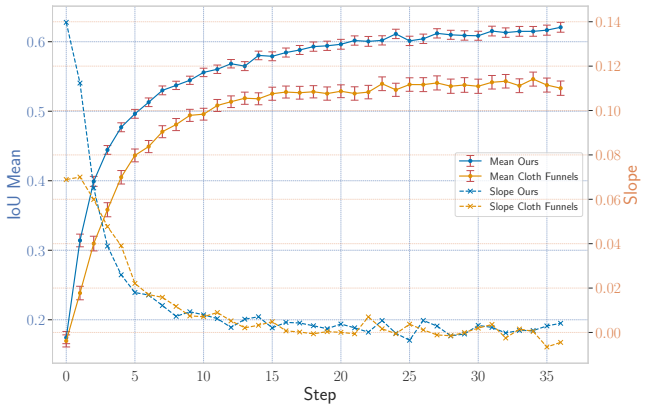

Fig. 10: Garment alignment experiment results. The slope indicates the increasing speed of the IoU Mean values.

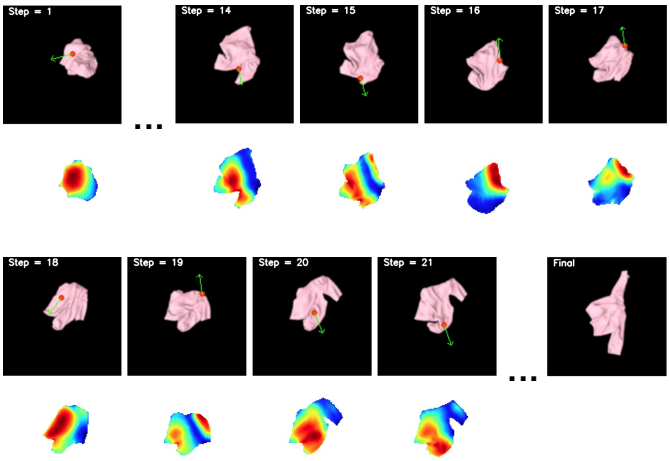

Fig. 11: The visualizations of the garment alignment task, with a predefined goal of the neck pointing right.

wrinkle generation by action in any direction. The angle map consistently shows a center location relative to the garment, with directions pointing toward the edge that is determined by the garment mask. This alignment is consistent with the basic rule of garment unfolding. Furthermore, the densely distributed actions, indicated by white arrows, tend to point from the center toward the edges of the garment, clearly demonstrating their effectiveness in radiating the garment.

Furthermore, we show the complete unfolding process of our model for two garment types, long sleeves and dress, in Fig. 9. The actions for both types of garments are generated by the same model. Although the model was trained on isolated samples, the unfolding sequences demonstrate its potential for long-horizon manipulation. In the initial steps, the garments are heavily crumpled, and the model produces actions that roughly unfold the outer edges to increase the overall coverage area. As key regions such as corners, hems, and necklines become exposed, the model progressively shifts its focus to those areas, generating finer actions to eliminate small wrinkles.

In addition to unfolding tasks, we also evaluate our methods by alignment tasks, where the objective is to position the garment into a specific target pose while unfolding. The target position is fixed and placed in the center of the image, with the collar or waistband pointing to the right. The employed metric is the widely adopted IoU value as the alignment index, which quantifies the similarity between the final state and the target configuration. The higher the alignment index value, the closer the garment is to the target pose.

We plot the IoU value after each "pull" action, as shown in Fig. 10. Our method exhibits a steeper increase in IoU during the early stages compared to the spatial action map method [10]. While both methods eventually converge to stable states where further actions have little impact on the garment configuration, our approach achieves a higher final IoU value, indicating superior alignment performance.

We present the visualization of the actions and the corresponding score maps in Fig. 11. With the same model structure, the generated actions and the score maps exhibit

TABLE IV: Ablation Study Results for the Score Map Training

Virant	SEBlock	Action Enlarging	Background Information	Coverage	Relative Increase
(a)				0.812	0.00
(b)	✓			0.817	0.62
(c)		✓		0.821	1.11
(d)			✓	0.816	0.49
(e)	✓	✓		0.844	3.94
(f)	✓		✓	0.825	1.60
(g)		✓	✓	0.845	4.06
(h)	✓	✓	✓	0.854	5.17

different patterns compared to the unfolding tasks shown in Fig. 9. Specifically, the key region of the score map is not limited to the edge of the garment, but includes the center areas, enabling large whole-body transformation during alignment. The goal of the action varies across different stages according to the state of the garment. For example, in Fig. 11, in the early stage (before Step 14), the actions mainly focus on unfolding the garment. Then, in the latter stages, the actions aim to rotate and transform the garment to align it with the predefined target goals. Notably, these actions (Step 15 to Step 21) may slightly fold the garment and create wrinkles, which demonstrates a shift in strategy as the process evolves.

B. Ablation Study

The specially proposed modules for garment manipulation tasks include the incorporation of the SEBlock, enlargement of the action area, fusion of background information, and the proposed shape loss for the alignment task. We perform systematic ablation experiments to evaluate module effectiveness and uncover their working principles.

1) Score map training: First, the SEBlock is incorporated into the score head that predicts the score map to reweight the feature maps channel-wise. Then, two methods are proposed to improve the score loss training, i.e., the action field enlargement and the background information fusion. These two methods address the imbalance between the foreground and background, each from a unique perspective: one by enlarging the action area and the other by incorporating background information.

We conduct ablation studies on the score head modules using the unfolding task, where the architecture preserves the complete scoring mechanism without interference from the supplementary components present in the alignment task. In Table IV, we present the results for the "long sleeves" clothing type, shown progressively. The variants range from the vanilla model to the full model that contains all the modules.

In Table IV, our vanilla model, which lacks any designed modules for score training, still achieves a higher coverage index than the state-of-the-art method reported by [10]. This result highlights the effectiveness of the overall dense action generator, demonstrating superior performance compared to the spatial action map method. This superiority may be attributed to the model's ability to continuously predict action parameters, i.e., angle and distance. In addition, in Table IV, the coverage index values show a progressive increase with

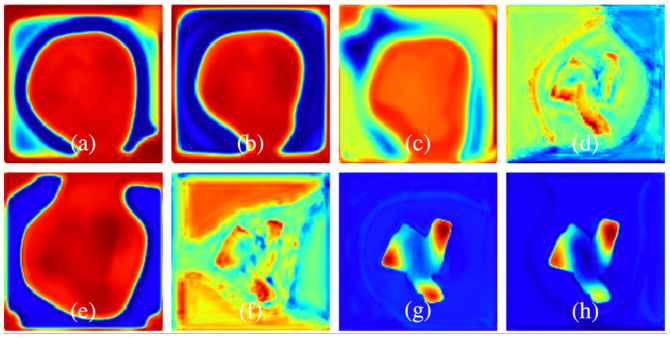

Fig. 12: Score map comparison of each model variant in ablation study.

sequential integration of the designed modules. Compared to the vanilla model, each of the three variants that incorporate individual modules independently improves the results, with relative increases ranging from 0.49% to 1.11%. These results demonstrate that the proposed modules can independently enhance the accuracy of score map prediction. The *Action Enlarging* module achieves the highest relative increase. Furthermore, with a combination of the two proposed modules, the accuracy improves further compared to variants with a single module, with increases between 1.60% and 4.06%, indicating that the modules do not interfere with each other. Ultimately, the complete model achieves the highest accuracy, marking a significant relative increase of 5.17% over the vanilla model.

Furthermore, Fig. 12 presents the score maps for each of the models in the ablation experiment. Compared with images (d) and (f)-(h), which have background information integration, images (a)-(c) and (e) erroneously highlight the background, especially at the edge and corner areas, and fail to clearly output the contour of the garment. This suggests a potential overfitting issue due to an information imbalance between foreground and background. Then, comparing image (d) to images (g) and (h), it shows that only the background information module still struggles to capture high-accuracy semantic details. However, the addition of an action enlarging module significantly reduces noise and clarifies the garment contours, indicating that the combination of these two modules effectively learns semantic information. Notably, the model automatically and precisely retrieves the manipulation areas, i.e., corner areas in the case of the garment unfolding task, which aligns with common practices of unfolding a garment with single-point interaction. Finally, when comparing images (g) and (h), the SEBlock module appears to guide the model to focus on the most important areas, further refining the score map.

Although it is not feasible to completely decouple the modules for isolated effectiveness evaluation due to interdependencies during training, (e.g., weight equilibrium perturbations), our targeted module isolation protocol through progressive ablation still reveals measurable performance gains across components. The results in Table IV show that all proposed modules contribute to enhancing the accuracy of the score.

Fig. 13: IoU values of the alignment task of the model trained with the shape loss.

TABLE V: Ablation Results on the Alignment Task

Variants	Shape Weights	IoU	
		Step10	Step36
(1)	0.0	0.482	0.536
(2)	1.0	0.506	0.557
(3)	10.0	0.530	0.612
(4)	25.0	0.560	0.621
(5)	100.0	0.537	0.573

2) Shape loss: The shape loss learns the action field that moves the pixels of the garment to the positions specified by the target state. For the evaluation of shape loss, we train the action generator with different shape loss contributions by adjusting the shape loss weight λ_s. We then employ the alignment index, IoU values, to quantitatively evaluate their performance. As shown in Fig. 13, the IoU values of the model with effective shape loss, i.e., with $\lambda_s \in [1.0, 10.0, 25.0, 100.0]$, are larger than that of the baseline model with no contributions from the shape loss, i.e., with a $\lambda_s = 0$, in most steps and ultimately stabilize, demonstrating the effectiveness of adopting shape loss. This also confirms the feasibility of simulating actions of the action field through pixel movements. Furthermore, the slopes of the IoU curves for the models with shape loss are larger than those of the vanilla model in the early stages, indicating that it is more effective when the garments' states are at greater discrepancies to the target and thus in a more challenging state. This might be because the shape loss model is also supervised by the target state, which is less influenced by the distances of the labeled actions. In contrast, the action field learned through the shape loss does not limit the scale of action, allowing for larger adjustments that quickly align the garment in the early stages.

To further investigate the impact of the proposed shape loss, we present the detailed evaluation results, as shown in Table V. The baseline model with $\lambda_s = 0.0$ records an IoU value of 0.482 after 10 steps of planar action, and it finally reaches 0.536 after 36 steps, illustrating the effectiveness of planar action in garment alignment. As the shape loss appears and its contribution gains with the λ_s increasing to 1.0, 10.0, and 25.0, the variants achieve higher IoU values in both Step10 and Step36, simultaneously and progressively. However, once the shape weight λ_s reaches 100.0, the IoU values of Step10 and Step36 fall back to 0.537 and 0.573. This suggests that an overemphasis on shape similarity may not optimally align with other critical factors, such as overall pose error. Thus, the contribution of sampled labels should also be balanced to achieve the highest IoU value.

While shape loss guides actions for higher overall IoU, it focuses solely on image-level similarity, neglecting detailed garment state information. Although specific and accurate, the shape loss is not directly and fully aligned with the alignment goal, which means that the final result of only shape loss potentially leads to a local minimum. For example, the garment may be in an opposite upside-down position. Meanwhile, each of the collected sampled actions manipulates the garment to a reduced average point-to-point distance, which gradually aligns the garment with the target pose. However, these sampled actions lack precise knowledge of the final target pose. Thus, balancing the contributions of shape loss and sampled action errors through a combined loss function, calculated as Equation (14), is crucial for achieving optimal garment alignment. Note that for the case when $\lambda_s = 100.0$, the shape loss contributes much more than the other regression losses, L_{angle} and $L_{distance}$, dominating the training of the model. This dominance suggests that the shape loss module can achieve the alignment task by itself, functioning as an unsupervised regression, which does not require other labels, i.e., gt_{sin}, gt_{cos}, and gt_l, to train the model.

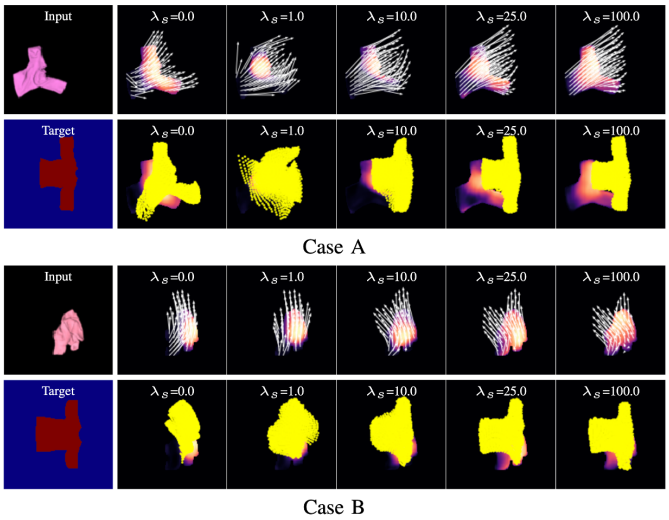

Fig. 14: Visualizing the impact of shape loss. Case A and Case B correspond to different initial states. For both cases, the top row displays the input image and the generated dense actions (white arrows) under different shape loss weights, while the bottom row displays target masks and the results of pixel movements (yellow dots) by these actions.

As described in Section III-C3, the movement of a single pixel determined by each of the dense actions can approximate the overall manipulation result. We provide visualization of actions and the image results in Fig. 14. The actions within the garment area are denoted with white arrows, and the ends of these arrows are marked as yellow dots for clear visualization of the pixel movement results. As shown in Case A of Fig. 14, when λ_s increases from 0.0 to 100.0, the model is more heavily supervised by the shape loss, making the resulting shape closer to the target mask. Specifically, without the shape loss ($\lambda_s = 0.0$), most of the actions have similar angles, which only have the effect of transforming the garment area. Then, as the weight λ_s increases from 0.0 to 1.0, the shape loss begins to occur and exerts its effect. Consequently, the overall result is that the dense pixel movements lead to an unfolding effect, which enlarges the size of the garment area. Finally, as the weight increases to a value such as $\lambda_s \in [10.0, 25.0, 100.0]$, the contours of the result areas are

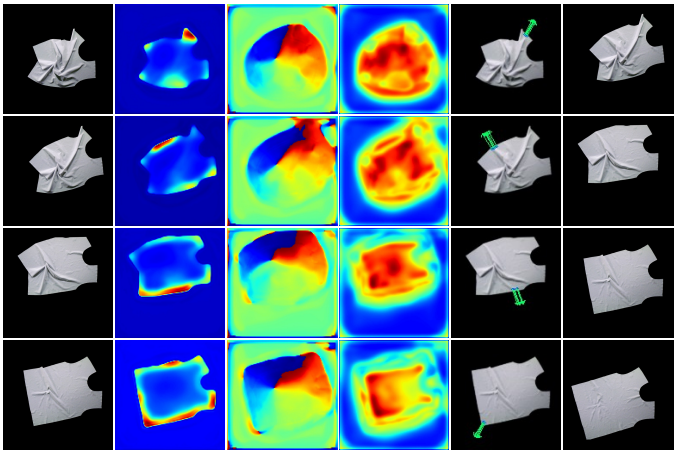

Fig. 15: Steps of a T-shirt-shaped fabric unfolding trial. From left to right, the images depict the initial state, score map, angle map, distance map, visualization of the action, and final state (which serves as the initial state for the next step). From top to bottom, each row represents a single step.

clearer and more similar to the target mask, compared with the results with $\lambda_s = [0.0, 1.0]$. This indicates that the model can generate actions that effectively manipulate the garment to align with the target. This observation is consistent with the quantitative results presented in Table V and elucidates the decline in the IoU when λ_s is excessively increased.

On the other hand, for Case B shown in Fig. 14, the trends in pixel movements with changes in λ_s are similar to the positive case, despite the differences in the initial pose compared to Case A. This suggests that our method employs a consistent strategy regardless of initial conditions. Therefore, the shape loss itself focuses solely on reducing the shape difference between the result and the target garment mask, which is at the image-level guidance. In other words, a model trained only with shape loss fails to retrieve the inner structure and semantic information from the garment image, and struggles with extreme poses. For this reason, shape loss requires the integration with the supervised learning of the angle and distance.

C. Real-world Experiments

To further evaluate the effectiveness of the proposed robot garment manipulation system and assess the simulation-to-real gap, we conduct real-world experiments using our network trained only on simulated data. We tested the system on seven different upper garments, including vests, T-shirts, and long sleeves. Each garment contains 5 trials in which the garment is manipulated from randomly crumpled states by the robot. A trial is stopped when the coverage index is stable in consecutive actions or reaches a maximum of 10 actions. The results are present in Table VI. It can be observed that the models trained solely by the synthetic garment images in the simulator demonstrate high coverage indexes in the real-world experiment. Compared with Cloth Funnels [10], the robot with our action generator achieves higher coverage index values

TABLE VI: Real-world Garment Unfolding Experiment

Methods	Coverage	
	Step3	StepFinal
Cloth Funnels [10]	0.814	0.833
Ours	0.851	0.865

after the first 3 actions (Step3) and when the trial is stopped (StepFinal), further demonstrating its superior performance.

Fig. 15 presents an example of a real-world unfolding sequence, with each row showing the fabric state after executing one pulling action. The first column shows the captured fabric scene, which is sent to the action generation model to produce a 3-channel image, comprising the score, angle, and distance map, shown in columns 2 to 4, respectively. The dense actions are then reconstructed by these 3-channel images. The actions with the top 5 highest scores are displayed in column 5. Finally, the robot arm executes the action with the highest score, and the final state of the fabric is shown in column 6. This final state also serves as the initial state for the next step. As shown in Fig. 15, our robotic system can progressively unfold crumpled fabric in a real-world environment. The distance map highlights fabric regions that require longer pulling actions. By applying the "pull" action indicated by green arrows, the fabric gradually becomes smoother and less wrinkled. Through multiple steps, the fabric is completely flattened, demonstrating our system's potential for real-world deployment with minimal adaptation.

Fig. 16 shows examples of the experimental results using different garment types, including T-shirts and long sleeves. Our model achieves good unfolding performance on the novel T-shirts and long sleeves. The score maps demonstrate that the model can consistently highlight appropriate pulling start regions for manipulation and adjust the score distribution according to the current garment configuration. We also provide supplementary videos to demonstrate the experiments.

V. Conclusion

In this paper, we propose a robotic system capable of automatically manipulating various categories of garments. The vision-based generation model is specifically designed for the single-point planar action. We introduce a novel framework to generate dense actions by single model forward propagation, significantly reducing the computation time while ensuring the prediction of continuous action parameters. For action score generation, we identify class imbalance as the primary cause of performance degradation and suggest incorporating the background semantic information to address this issue. Furthermore, we leverage target masks and shape similarity metrics to guide the model training, enhancing manipulation accuracy without additional computational overhead. Extensive experiments in both simulated and real-world environments demonstrate the superior performance of our method.

References

[1] J. Luo, C. Xu, X. Geng, G. Feng, K. Fang, L. Tan, S. Schaal, and S. Levine, "Multi-stage cable routing through hierarchical imitation learning," *IEEE Transactions on Robotics*, 2024.

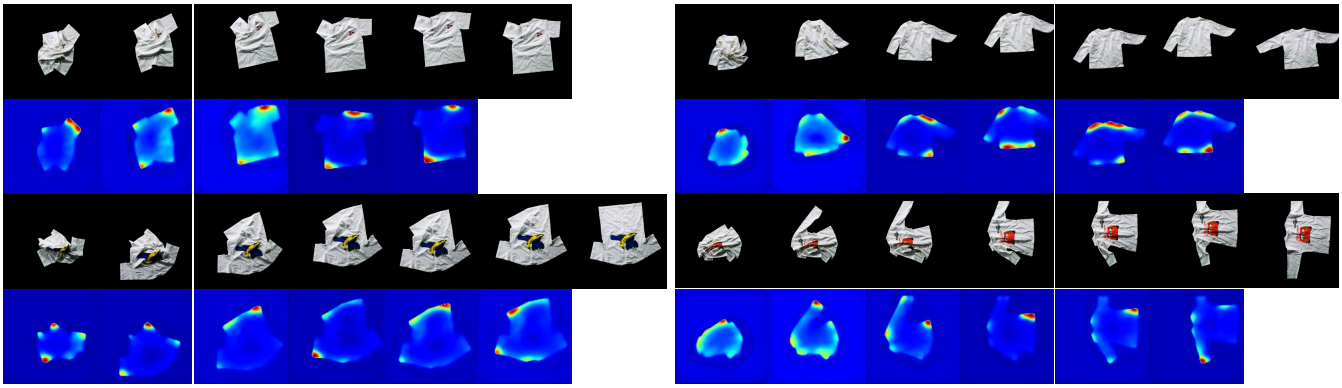

(a) T-shirt (b) Long sleeves

Fig. 16: Selected results of the garment unfolding experiment of the T-shirts and long sleeves. Each trial would be terminated early if the coverage index value stabilizes or reaches a threshold.

[2] L. Y. Chen, B. Shi, D. Seita, R. Cheng, T. Kollar, D. Held, and K. Goldberg, "Autobag: Learning to open plastic bags and insert objects," in *2023 IEEE International Conference on Robotics and Automation (ICRA)*. IEEE, 2023, pp. 3918–3925.

[3] Y. Li, Y. Wang, Y. Yue, D. Xu, M. Case, S.-F. Chang, E. Grinspun, and P. K. Allen, "Model-driven feedforward prediction for manipulation of deformable objects," *IEEE Transactions on Automation Science and Engineering*, vol. 15, no. 4, pp. 1621–1638, 2018.

[4] X. Huang, A. Seino, F. Tokuda, A. Kobayashi, D. Chen, Y. Hirata, N. C. Tien, and K. Kosuge, "Sis: Seam-informed strategy for t-shirt unfolding," *arXiv preprint arXiv:2409.06990*, 2024.

[5] C. Zhou, H. Xu, J. Hu, F. Luan, Z. Wang, Y. Dong, Y. Zhou, and B. He, "Ssfold: Learning to fold arbitrary crumpled cloth using graph dynamics from human demonstration," *IEEE Transactions on Automation Science and Engineering*, vol. 22, pp. 14 448–14 460, 2025.

[6] P. Sundaresan, J. Grannen, B. Thananjeyan, A. Balakrishna, M. Laskey, K. Stone, J. E. Gonzalez, and K. Goldberg, "Learning rope manipulation policies using dense object descriptors trained on synthetic depth data," in *2020 IEEE International Conference on Robotics and Automation (ICRA)*. IEEE, 2020, pp. 9411–9418.

[7] C. Chi and S. Song, "Garmentnets: Category-level pose estimation for garments via canonical space shape completion," in *Proceedings of the IEEE/CVF International Conference on Computer Vision*, 2021, pp. 3324–3333.

[8] Y. Deng and D. Hsu, "General-purpose clothes manipulation with semantic keypoints," *arXiv preprint arXiv:2408.08160*, 2024.

[9] H. Ha and S. Song, "Flingbot: The unreasonable effectiveness of dynamic manipulation for cloth unfolding," in *Conference on Robot Learning*. PMLR, 2022, pp. 24–33.

[10] A. Canberk, C. Chi, H. Ha, B. Burchfiel, E. Cousineau, S. Feng, and S. Song, "Cloth funnels: Canonicalized-alignment for multi-purpose garment manipulation," in *2023 IEEE International Conference on Robotics and Automation (ICRA)*. IEEE, 2023, pp. 5872–5879.

[11] L. Yang, Y. Li, and L. Chen, "Clothppo: a proximal policy optimization enhancing framework for robotic cloth manipulation with observation-aligned action spaces," in *Proceedings of the Thirty-Third International Joint Conference on Artificial Intelligence*, 2024, pp. 6895–6903.

[12] C. Zhou, R. Jiang, F. Luan, S. Meng, Z. Wang, Y. Dong, Y. Zhou, and B. He, "Dual-arm robotic fabric manipulation with quasi-static and dynamic primitives for rapid garment flattening," *IEEE/ASME Transactions on Mechatronics*, pp. 1–11, 2025.

[13] A. Zeng, S. Song, S. Welker, J. Lee, A. Rodriguez, and T. Funkhouser, "Learning synergies between pushing and grasping with self-supervised deep reinforcement learning," in *2018 IEEE/RSJ International Conference on Intelligent Robots and Systems (IROS)*. IEEE, 2018, pp. 4238–4245.

[14] T. Schmidt, R. Newcombe, and D. Fox, "Self-supervised visual descriptor learning for dense correspondence," *IEEE Robotics and Automation Letters*, vol. 2, no. 2, pp. 420–427, 2016.

[15] H. Cheng, Y. Wang, and M. Q. H. Meng, "Anchor-based multi-scale deep grasp pose detector with encoded angle regression," *IEEE Transactions on Automation Science and Engineering*, vol. 21, no. 3, pp. 3130–3142, 2024.

[16] A. Ganapathi, P. Sundaresan, B. Thananjeyan, A. Balakrishna, D. Seita, J. Grannen, M. Hwang, R. Hoque, J. E. Gonzalez, N. Jamali *et al.*, "Learning dense visual correspondences in simulation to smooth and fold real fabrics," in *2021 IEEE International Conference on Robotics and Automation (ICRA)*. IEEE, 2021, pp. 11 515–11 522.

[17] R. Wu, H. Lu, Y. Wang, Y. Wang, and H. Dong, "Unigarmentmanip: A unified framework for category-level garment manipulation via dense visual correspondence," in *Proceedings of the IEEE/CVF Conference on Computer Vision and Pattern Recognition*, 2024, pp. 16 340–16 350.

[18] D. Berenson, "Manipulation of deformable objects without modeling and simulating deformation," in *2013 IEEE/RSJ International Conference on Intelligent Robots and Systems*. IEEE, 2013, pp. 4525–4532.

[19] Y. Wu, W. Yan, T. Kurutach, L. Pinto, and P. Abbeel, "Learning to manipulate deformable objects without demonstrations," in *Robotics: Science and Systems*, 2020.

[20] J. Matas, S. James, and A. J. Davison, "Sim-to-real reinforcement learning for deformable object manipulation," in *Conference on Robot Learning*. PMLR, 2018, pp. 734–743.

[21] X. Lin, Y. Wang, Z. Huang, and D. Held, "Learning visible connectivity dynamics for cloth smoothing," in *Conference on Robot Learning*. PMLR, 2022, pp. 256–266.

[22] W. Wang, G. Li, M. Zamora, and S. Coros, "Trtm: Template-based reconstruction and target-oriented manipulation of crumpled cloths," in *2024 IEEE International Conference on Robotics and Automation (ICRA)*. IEEE, 2024, pp. 12 522–12 528.

[23] Z. Huang, X. Lin, and D. Held, "Mesh-based dynamics with occlusion reasoning for cloth manipulation," in *Robotics: Science and Systems (RSS)*, 2022.

[24] V. Raval, E. Zhao, H. Zhang, S. Nikolaidis, and D. Seita, "Gpt-fabric: Folding and smoothing fabric by leveraging pre-trained foundation models," *arXiv preprint arXiv:2406.09640*, 2024.

[25] J. Shi *et al.*, "Good features to track," in *1994 Proceedings of IEEE conference on computer vision and pattern recognition*. IEEE, 1994, pp. 593–600.

[26] J. Achiam, S. Adler, S. Agarwal, L. Ahmad, I. Akkaya, F. L. Aleman, D. Almeida, J. Altenschmidt, S. Altman, S. Anadkat *et al.*, "Gpt-4 technical report," *arXiv preprint arXiv:2303.08774*, 2023.

[27] A. B. Clark, L. Cramphorn-Neal, M. Rachowiecki, and A. Gregg-Smith, "Household clothing set and benchmarks for characterising end-effector cloth manipulation," in *2023 IEEE International Conference on Robotics and Automation (ICRA)*. IEEE, 2023, pp. 9211–9217.

[28] W. Chen, D. Lee, D. Chappell, and N. Rojas, "Learning to grasp clothing structural regions for garment manipulation tasks," in *2023 IEEE/RSJ International Conference on Intelligent Robots and Systems (IROS)*. IEEE, 2023, pp. 4889–4895.

[29] T. Weng, S. M. Bajracharya, Y. Wang, K. Agrawal, and D. Held, "Fabricflownet: Bimanual cloth manipulation with a flow-based policy," in *Conference on Robot Learning*. PMLR, 2022, pp. 192–202.

[30] M. Agarwal, T. Weng, and D. Held, "Point-based correspondence estimation for cloth alignment and manipulation," in *RSS 2023 Workshop on Symmetries in Robot Learning*.

[31] J. Wu, X. Sun, A. Zeng, S. Song, J. Lee, S. Rusinkiewicz, and

T. Funkhouser, "Spatial action maps for mobile manipulation," *arXiv preprint arXiv:2004.09141*, 2020.

[32] Z. Xu, C. Chi, B. Burchfiel, E. Cousineau, S. Feng, and S. Song, "Dextairity: Deformable manipulation can be a breeze," *arXiv preprint arXiv:2203.01197*, 2022.

[33] D. Blanco-Mulero, G. Alcan, F. J. Abu-Dakka, and V. Kyrki, "Qdp: Learning to sequentially optimise quasi-static and dynamic manipulation primitives for robotic cloth manipulation," in *2023 IEEE/RSJ International Conference on Intelligent Robots and Systems (IROS)*. IEEE, 2023, pp. 984–991.

[34] C. Gao, Z. Li, H. Gao, and F. Chen, "Iterative interactive modeling for knotting plastic bags," in *Conference on Robot Learning*. PMLR, 2023, pp. 571–582.

[35] K. He, X. Zhang, S. Ren, and J. Sun, "Deep residual learning for image recognition," in *Proceedings of the IEEE conference on computer vision and pattern recognition*, 2016, pp. 770–778.

[36] J. Hu, L. Shen, and G. Sun, "Squeeze-and-excitation networks," in *Proceedings of the IEEE conference on computer vision and pattern recognition*, 2018, pp. 7132–7141.

[37] X. Lin, Y. Wang, J. Olkin, and D. Held, "Softgym: Benchmarking deep reinforcement learning for deformable object manipulation," in *Conference on Robot Learning*. PMLR, 2021, pp. 432–448.

[38] Y. Li, J. Wu, R. Tedrake, J. B. Tenenbaum, and A. Torralba, "Learning particle dynamics for manipulating rigid bodies, deformable objects, and fluids," in *International Conference on Learning Representations*, 2019.